

UHF Propagation in Indoor Hallways

Dana Porrat and Donald C. Cox, *Fellow, IEEE*

Abstract—A new model for UHF propagation in large buildings is presented. This model relies on knowledge of the interior arrangement of the building without requiring much detail. The guiding of radiation along hallways is the most significant propagation process at distances of more than 10 m from the transmitter. The waveguide model predicts the power loss rate along the hallways, which is affected by the coupling among the propagating modes. The coupling results from the roughness of the surfaces in the building; it is predicted in an average manner using the average deviation of the walls from perfect smoothness. The model predictions are compared to measurements in an office building and to ray tracing predictions.

Index Terms—Indoor propagation, multimode waveguide, radio channel modeling, UHF radio.

I. INTRODUCTION

THE understanding of indoor radio propagation is important in the design and layout of mobile data and voice systems. A good model should provide insights into the propagation mechanism, in addition to predicting power levels throughout the building. Current models of propagation in the UHF band (300 MHz–3 GHz) are based on ray tracing, with strong diffraction effects [1]–[4], or on empirical distance power laws [5].

Ray tracing provides reasonably accurate prediction of power levels, when detailed information on the geometry and materials of the building is available. It is less useful when an overall picture is needed of the propagation, or when the geometry of the building is given without much detail.

Measurements show that despite the relative transparency of wall materials, hallway guidance is the most significant propagation mechanism at medium and large distances from the source (starting at a radius of about 10 m). Waveguide models were suggested for hallways by Kyritsi and Cox [6], but these models assume perfectly smooth walls, with no mode coupling. In this paper, we suggest a more sophisticated model, that takes into account coupling among the waveguide modes, caused by the roughness of the walls. We investigate the effect of coupling on power levels in a building, in the hallways, and adjacent rooms. Our model offers insight into commonly observed phenomena, in particular the effect of hallway junctions, on measured power levels.

The advantage offered by the waveguide modeling approach over existing methods (namely ray tracing and power laws)

is an overall picture of power levels in a large area with very small computational and database requirements. The model requires very little detailed information about the environment and provides accurate predictions of the major phenomena. The input parameters used by the model are few and describe the construction of walls in an average way, and the geometrical description is very simple. The prediction of power levels is accurate, in particular the levels predicted near hallway junction. In contrast, ray tracing requires detailed information about the environment in order to produce comparable predictions. Ray tracing algorithms are also much more complicated and require larger computer resources than the waveguide model. Power Law models are simple and computationally very light, but they do not supply predictions that depend on the specifics of the structures. In particular, it is hard to model the effect of hallway junctions using this approach.

The measurement results are presented in Section II, followed by the model in Section III, and discussion and detailed comparison to ray tracing in Section IV.

II. MEASUREMENTS

The measurements were taken in the basement of an office building, where interference is low. Many modern office buildings are built with concrete and metal slabs between floors, so we expect that the propagation phenomena in hallways above ground in these buildings would be similar to the ones shown here.

Measurements were taken in the 850–950-MHz band, in the Packard building in Stanford University. The power was measured with a 250-kHz resolution, with an accuracy of 1 dB. The antennas were quarter-wave monopole with a magnetic mount, standing over a 0.3×0.3 m² ground plane.

A. Measurement Setup

The setup consisted of two polyethylene carts which were placed in the hallways or the rooms. One cart held the transmitting antenna and the other the receiving antenna and other equipment. A diagram of the setup is shown in Fig. 1. The source was the tracking generator of the HP8595E spectrum analyzer and the computer was used to record the received power spectra.

B. Environment

The Packard building is an office and laboratory building in the Stanford University campus, built around 1999. The ceiling is floating, with metal plates between the top of the basement and the ground floor of the building, and the floor is concrete. The interior walls are mostly drywall, 5/8 in thick on each side, with aluminum studs 2 × 4 in, at 16-in separations, some walls are reinforced with concrete.

Manuscript received June 3, 2002; revised February 24, 2003; accepted May 5, 2003. The editor coordinating the review of this paper and approving it for publication is R. Valenzuela.

D. Porrat is with the University of California at Berkeley, Berkeley, CA 94703 USA (e-mail: dporrat@wireless.stanford.edu).

D. C. Cox is with Stanford University, Stanford, CA 94305 USA (e-mail: dcox@spark.stanford.edu).

Digital Object Identifier 10.1109/TWC.2004.828023

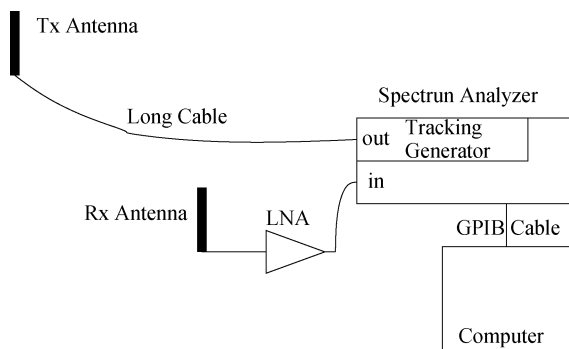


Fig. 1. Measurement setup.

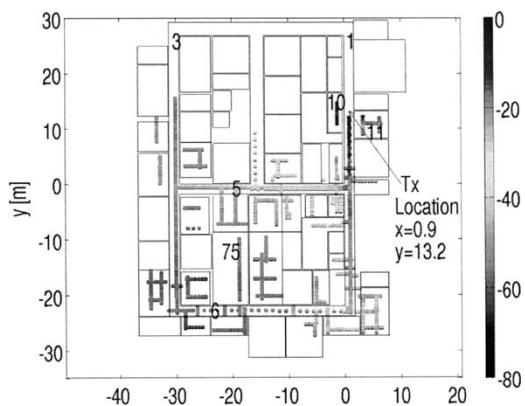


Fig. 2. Locations of the transmitter and receiver in the Packard basement, with median power level at each receiver location (decibels). The single digit numbers indicate hallways and the two-digit numbers indicate rooms in the building. The lines indicate the inner boundary of the hallway and room walls. Details of the walls and doors were omitted.

1) *Measurement Locations:* Measurements were taken in the hallways and rooms of the basement of the Packard building. Most of the measurements were taken with the transmitter at one location and the receiver moving in the building. Fig. 2 shows the locations of the transmitter and the receiver for the relevant measurements, with the median power level at each receiver location. The locations were usually measured accurately (within 10 cm) in the hallways, but the locations in the room have lower accuracy. As a result, some measurements in Fig. 2 appear to be on the walls.

C. Results

This section shows median power levels measured along the hallways and in adjacent rooms. The median power level over the band (850–950 MHz) is shown for each measurement location. Taking the median over the frequency band has a similar effect as taking a median over single frequency measurements over a small (spatial) neighborhood. The median was used instead of a mean in order to reduce the effect of deep fades on the result. For most measurements, the median is close to the mean (taken over frequency); specifically, the median is between mean $- 0.5$ dB and mean $+ 1.5$ dB in 92% of the measurements. The sensitivity of the receiver was around $- 90$ dB, where the limitation is leakage from the connector of the cable linking the generator to the transmitting antenna.

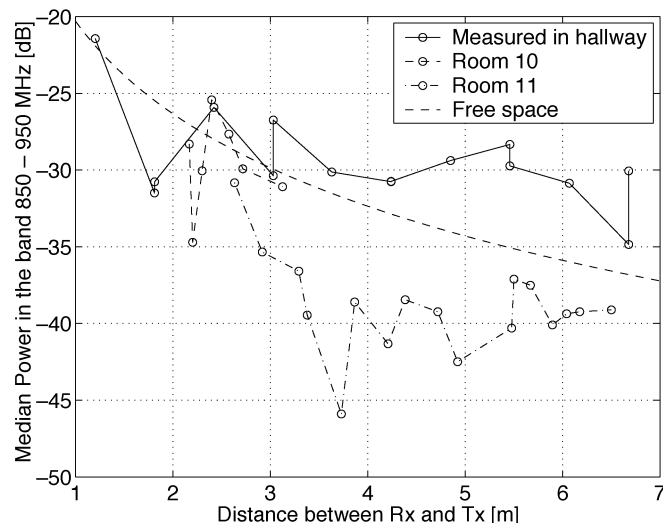


Fig. 3. Power received near the transmitter; the geometry is shown in Fig. 2. The free-space curve is an estimation based on measurements at close range.

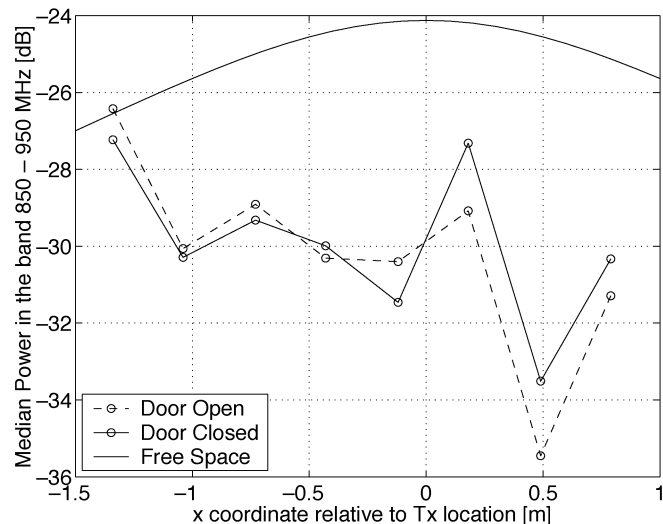


Fig. 4. Power received across a wall; the geometry is shown in Fig. 5. The free-space curve is an estimation based on measurements at close range.

1) *Wall Penetration:* Fig. 3 shows the power received in the near environment of the transmitter in the hallway and in two adjacent rooms. The geometry is shown in Fig. 2. The measurements in room 11 show considerably lower power than room 10 and the reason is concrete wall separating room 11 from the hallway. In room 10, power levels are very similar to the hallway level. The difference is within the accuracy margin of our measurements, that is limited by temporal variations and the inaccuracy of the equipment. A reliable estimate of the drywall attenuation cannot be obtained from our measurements, except to say that the penetration is very good. Measurements in [7] and [8] show attenuation of 0.1–0.5 dB for perpendicular incidence on drywall boards of various widths.

Another indication of the penetration through drywall is shown in Fig. 4, that presents the power measured along the wall of room 75, with the wooden door (more than 1.5 in thick) open and closed. The geometry of this measurement is shown in Fig. 5. The state of the door (open or closed) hardly affects

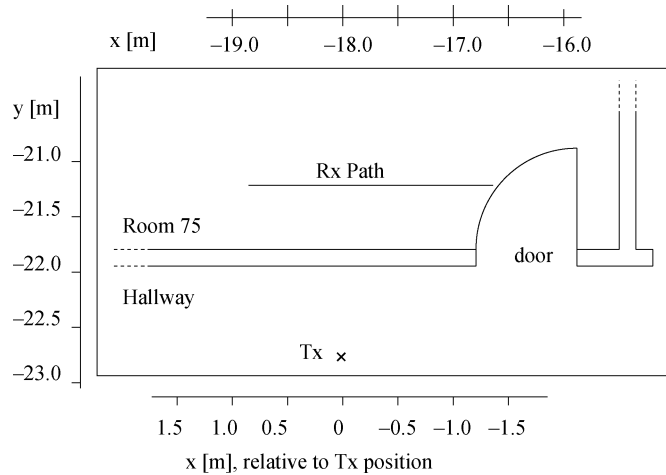


Fig. 5. Geometry of the measurements near room 75.

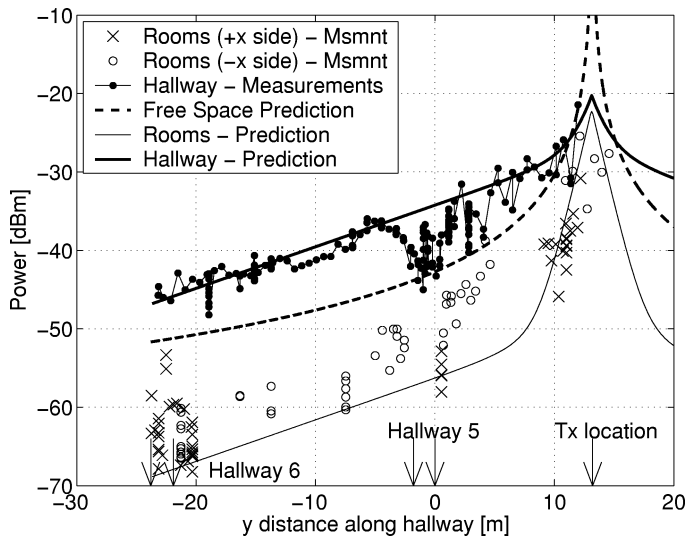


Fig. 6. Median power in Hallway 1 and adjacent rooms. The hallway data are at points 0.5 m or more from both walls. The room data are at points between 1 and 5 m from one of the hallway walls. The geometry is shown in Fig. 2. Model parameters are $\epsilon = 3$, $\sigma = 0.035$ S/m, $D = 2$ m, $s^2 = 0.2$ m², and the hallway width is 1.8 m. The power distribution at the transmitter is a TE narrow source in the middle of the hallway.

the power levels. The door material is a significant obstacle for UHF radiation [5], so our conclusion is that most of the radiation penetrates directly through the wall.

Although penetration through the walls is very strong, the measurements shown below indicate that propagation via the hallways is a very important mechanism, when incidence on the walls is not normal.

2) *Power In and Near the Hallways:* Fig. 6 shows the power measured in Hallway 1 and the power measured in the adjacent rooms, at distances up to 5 m from the hallway. Hallway 1 contained the transmitter so locations in it, which have line of sight to the transmitter, receive more power than locations in the rooms. The theoretical curves in Fig. 6 are discussed in Section III.

One phenomenon seen in Hallway 1 is the increasing difference between the hallway power levels and the room power levels, at increasing distances from the transmitter. At locations

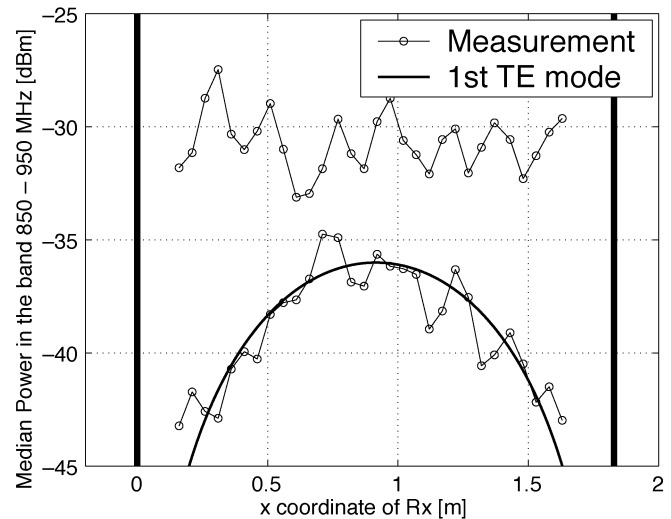


Fig. 7. Power across Hallway 1 (median over band). (Top) The receiver is 4.4 m from the transmitter. (Bottom) The receiver is 12 m from the transmitter. The vertical lines indicate the inner boundary of the hallway walls.

close to the transmitter, the difference in power levels is small (0 dB for the negative x and about 5 dB for the positive x). The walls in the positive x side are concrete in this area. At large distances from the transmitter, the difference between the hallway and the room levels is in the order of 15–20 dB for both sides.

The power levels in the hallway appear to be affected by the junction with Hallway 5, that is located between $y = 0$ and $y = -1.8$ m. Power levels *increase* from $y = -2$ to $y = -6$ m as the receiver moves away from the transmitter in Hallway 1, past the junction. Similar phenomena were measured in another building, but have not yet been explained in a satisfactory manner.

Power level variations across Hallway 1 were measured at various distances from the transmitter. Fig. 7 shows the median power at points across the hallway, with the receiver 4.4 and 12 m from the transmitter. Measurements done in the same hallway for larger distances show a shape similar to the bottom graph in Fig. 7, with higher levels received in the center of the hallway. Measurements in other hallways (with the transmitter still in Hallway 1) did not show a similar pattern.

The power in and near Hallway 5 is shown in Fig. 8, where the transmitter was located in Hallway 1. As in Hallway 1, the power levels in the rooms are similar to the levels in the hallway in the area closest to the transmitter (right of figure), with the difference growing as the receiver moves away from the transmitter. The difference between the hallway levels and the room levels is small for the rooms in the positive y side. The power level in the rooms on both sides of the hallway is similar for distances bigger than about 20 m from the junction with Hallway 1.

Another important effect is the sharp decrease of power levels at areas near the junction and the considerably lower rate of power loss at areas further from the transmitter.

The power along and near Hallway 6 is shown in Fig. 9, where the transmitter was located in Hallway 1. The strongest power levels in Hallway 6 were measured in the junction with Hallway 1. The power levels in the rooms are lower than those measured in the hallway, even for rooms on the positive y side

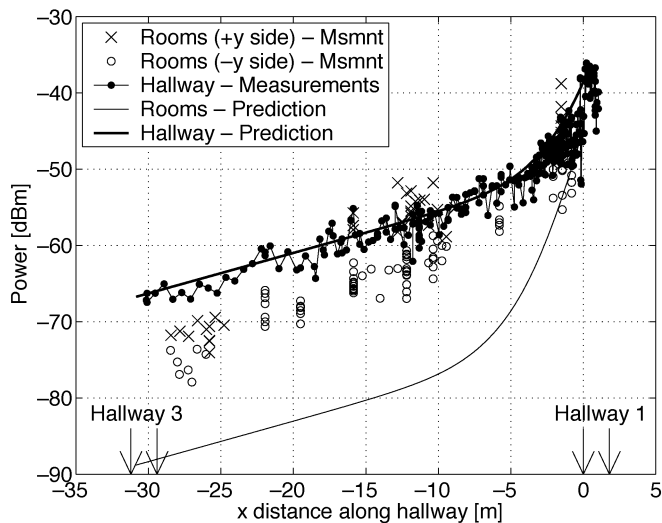


Fig. 8. Median power in Hallway 5 and adjacent rooms. The hallway data are at points 0.5 m or more from both walls. The room data are at points between 1 and 5 m from one of the hallway walls. The geometry is shown in Fig. 2. Model parameters are $\epsilon = 3$, $\sigma = 0.035$ S/m, $D = 2$ m, $s^2 = 0.2$ m², and the hallway width is 1.8 m. The power distribution at the junction is uniform.

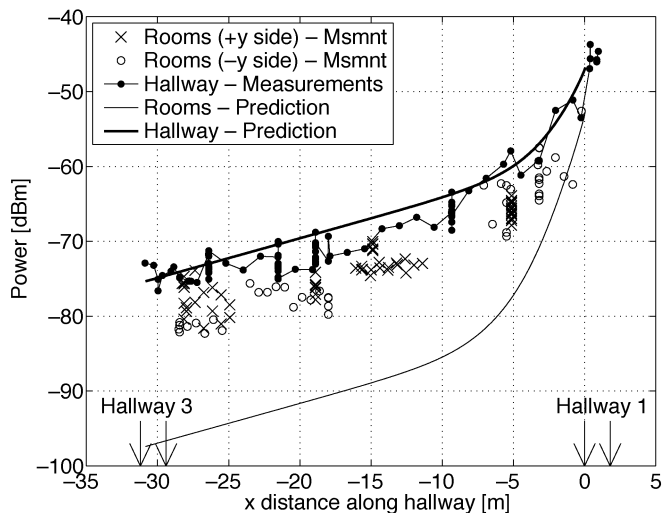


Fig. 9. Median power in Hallway 6 and adjacent rooms. The hallway data are at points 0.5 m or more from both walls. The room data are at points between 1 and 5 m from one of the hallway walls. The geometry is shown in Fig. 2. Model parameters are $\epsilon = 3$, $\sigma = 0.035$ S/m, $D = 2$ m, $s^2 = 0.2$ m², and the hallway width is 1.8 m. The power distribution at the junction is uniform.

of the hallway, which are closer to the transmitter. The power levels measured in the rooms in the positive y side for x between -25 and -30 m appear higher than those measured in the other side of the hallway. This may be an effect of the junction with Hallway 3, between $x = -29.1$ m and -30.9 m.

The power level and near Hallway 3 is shown in Fig. 10, where the transmitter was located in Hallway 1. The highest power levels in this hallway were measured at the crossing with Hallway 5 (between $y = 0$ and $y = 1.8$ m). An increase of power levels is evident also at the crossing with Hallway 6 (near $y = -23$ m).

High power levels are apparent in the rooms in both sides of the hallway, for positive y . The high power level measured

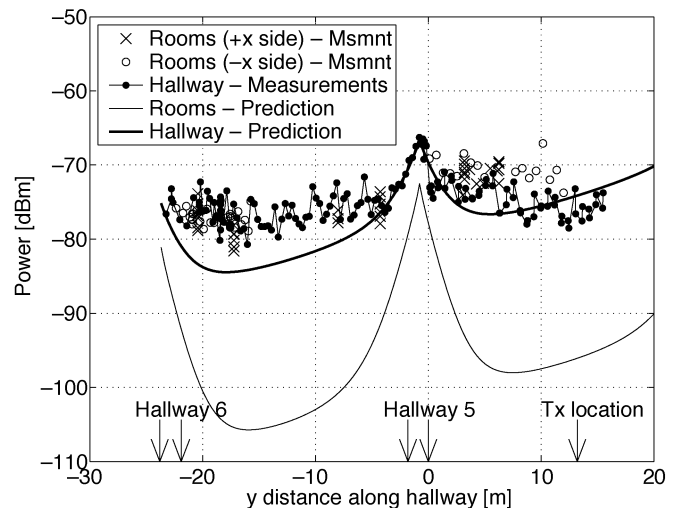


Fig. 10. Median power in Hallway 3 and adjacent rooms. The hallway data are at points 0.5 m or more from both walls. The room data are at points between 1 and 5 m from one of the hallway walls. The geometry is shown in Fig. 2. Model parameters are $\epsilon = 3$, $\sigma = 0.035$ S/m, $D = 2$ m, $s^2 = 0.2$ m², and the hallway width is 1.8 m. The power distribution at the junction is uniform.

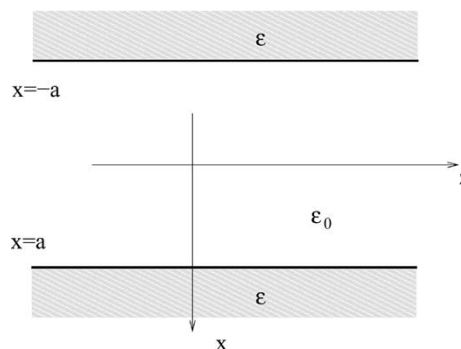


Fig. 11. Smooth slab waveguide.

on *both* sides of the hallway are not predicted by the theory. They may be partly explained by the normal incidence of direct propagation from the transmitter, that passes the intermediate walls with little loss.

III. MODEL

The model is presented here with some omission of details. For a complete development, see [9]. A waveguide model with smooth walls is discussed in Section III-A as a basis theory. This model is extended by considering rough (nonsmooth) walls in Section III-B. The waveguide model is two-dimensional (2-D) (it assumes no variation in the vertical direction), and the effects of the floor and ceiling are discussed in Section III-C.

A. Smooth Multimoded Waveguide

The simple model we present here consists of a slab waveguide. The walls of the waveguide are made of a lossy dielectric material (Fig. 11).

The waveguide is filled with air, so between the walls, we assume the electrical properties of free space. With this simple model, we ignore the effects of the floor and ceiling and any objects within the waveguide (such as people and furniture).

The waveguide can be defined in terms of its width and the relative complex dielectric constant of the walls ϵ

$$\epsilon_s(x, z) = \begin{cases} 1, & |x| \leq a \\ \epsilon, & |x| > a \end{cases} \quad (1)$$

where $\epsilon_s(x, z)$ stands for the relative dielectric constant of the smooth waveguide. The permeability is fixed at the vacuum value $\mu_0 = 4\pi \times 10^{-7}$ H/m for the walls and interior of the waveguide.

We are interested in multimoded waveguides because the normal width of hallways is many times the wavelength in the UHF band. We follow the waveguide analysis presented by Adam and Kneubühl [10] in the discussion of the smooth lossy hollow waveguide, and discuss a slab waveguide of width $2a$ with propagation along the z direction. There is no variation in the y direction. The lossy dielectric walls of the waveguide have the complex relative dielectric constant

$$\epsilon = \epsilon' + j\epsilon'' = \epsilon_r - j\frac{\sigma}{\omega\epsilon_0} \quad (2)$$

where ϵ_r is the relative permittivity of the walls, σ is their conductivity, ω is the angular frequency, $e^{j\omega t}$ is the time dependence, and $\epsilon_0 = 8.85 \times 10^{-12}$ F/m is the vacuum permittivity. A few other definitions: $k = 2\pi/\lambda$ is the free space wave number, where λ is the free space wavelength; β and $k_x = u/a$ represent the z and x components of the k vector for propagation inside the waveguide, where u is the normalized k vector in the x direction. $Z_0 = \sqrt{\mu_0/\epsilon_0}$ is the vacuum impedance, and \mathcal{H} and \mathcal{E} are arbitrary amplitudes.

The field expressions for the transverse electric (TE) modes inside the waveguide $|x| \leq a$ are brought from [10]

$$\mathbf{E} = E_y \hat{y} = j\frac{k}{k_x} Z_0 \mathcal{H} \begin{Bmatrix} \cos(k_x x) \\ \sin(k_x x) \end{Bmatrix} e^{j\omega t - j\beta z} \hat{y}. \quad (3)$$

The transverse magnetic (TM) modes

$$\mathbf{H} = H_y \hat{y} = -j\frac{k}{k_x} \frac{\mathcal{E}}{Z_0} \begin{Bmatrix} \cos(k_x x) \\ \sin(k_x x) \end{Bmatrix} e^{j\omega t - j\beta z} \hat{y}. \quad (4)$$

The upper functions in the curly braces apply to the symmetric modes and the lower to the antisymmetric modes, where the symmetry/antisymmetry characterizes the field component in the y direction. The field components not shown can be calculated using Maxwell's equations.

Using the boundary conditions, the characteristic equation can be formulated in terms of u , the propagation constant in the waveguide, and the properties of the waveguide. An exact solution of the characteristic equations is very difficult. Burke [11] gives a graphical solution for the TE case, but we follow [10] and discuss an approximate one. We assume that the imaginary parts of ϵ and u are small compared to their real parts. In order to test the assumption on ϵ , we calculate a typical value using the electrical properties of building materials: relative electrical permittivity $\epsilon_r = 4.44$ and conductivity $\sigma = 0.01$ S/m [12]. We consider radiation at 1 GHz and get $\epsilon = 4.44 - j0.18$, so the imaginary part is significantly smaller than the real part and the assumption on ϵ holds. The assumption on u relies on observing the solution obtained elsewhere (for example, in a graphical method).

Under these approximations on u and ϵ , the characteristic values of the real part of u (marked u') are as follows for the TE modes [10]:

$$u' = \pi(1 - \eta) \frac{n}{2} \quad (5)$$

where

$$\eta = \frac{\epsilon'' \lambda}{4\pi a (\epsilon' - 1)^{\frac{3}{2}}} \quad \text{and } n = 1, 2, \dots \quad (6)$$

and for the TM modes

$$u' = \pi(1 - \eta) \frac{n}{2} \quad (7)$$

where

$$\eta = \frac{\epsilon' + \frac{2\pi a}{\lambda} \epsilon'' (\epsilon' - 1)^{\frac{1}{2}}}{\left(\frac{2\pi a}{\lambda}\right)^2 (\epsilon' - 1)} \quad \text{and } n = 1, 2, \dots \quad (8)$$

Odd values of n correspond to the symmetrical modes and even values of n correspond to antisymmetric modes.

The propagation constant in the z direction is determined from $\beta^2 = k^2 - (u/a)^2$. By separating real and imaginary parts and neglecting terms of second degree we obtain the approximations for $\beta = \beta' + j\beta''$ [10]

$$\beta' = \left[\left(\frac{2\pi}{\lambda} \right)^2 - \left(\frac{u'}{a} \right)^2 \right]^{\frac{1}{2}}. \quad (9)$$

The imaginary part for the TE modes is given by

$$\beta'' = \frac{\lambda^2}{4a^3 (\epsilon' - 1)^{\frac{1}{2}}} \left(\frac{n}{2} \right)^2 \quad n = 1, 2, \dots \quad (10)$$

and for the TM modes

$$\beta'' = \frac{\epsilon' \lambda^2}{4a^3 (\epsilon' - 1)^{\frac{1}{2}}} \left(\frac{n}{2} \right)^2 \quad n = 1, 2, \dots \quad (11)$$

The number of significant modes N (for a single polarization) is determined by the condition $u' < ka$ and it can be approximated by $N \approx 2a/\lambda$ (assuming $\eta \ll 1$). When both TE and TM modes are considered, the number of significant modes is $2N$. In order to appreciate the number of propagating modes in the hallway waveguide, we calculate it for $a = 1$ m (the hallway width is 2 m) and $\lambda = 30$ cm (carrier frequency 1 GHz). We find $N = 6$ modes for each polarization.

1) *Power Carried by the Modes:* We calculate the power carried by the different modes, in order to normalize them at a later stage. The Poynting vector is given by

$$S = \frac{1}{2} \text{real}(\mathbf{E} \times \mathbf{H}^*) \quad (12)$$

and the power (per unit length in the y direction) is calculated by

$$P = \int_{-a}^a S_z dx \quad (13)$$

where we disregard the power propagating inside the walls of the waveguide. From this point on, we assume the convention

that the mode amplitudes \mathcal{H}_n and \mathcal{E}_n are normalized so that all the modes carry the same amount of power. We also assume that the modal amplitudes \mathcal{H}_n and \mathcal{E}_n are real and positive. When we consider later modes with different power levels or with complex amplitudes, we use a multiplicative coefficient for each mode.

2) *Orthogonality of the Modes:* We refer to two modes as orthogonal if the power carried by their combined fields when they propagate in the waveguide can be expressed as the sum of the powers carried by each mode separately for every location in the waveguide. If P_T is the total power measured in a waveguide and $\{P_n\}_{n=1}^N$ are the powers carried by N propagating modes, then these modes are orthogonal if at every point in the waveguide

$$P_T = \sum_{n=1}^N P_n. \quad (14)$$

A condition on mode orthogonality can be expressed in terms of the electric fields of the modes. Two modes are orthogonal if

$$I_{nm} = \int_{-a}^a \mathbf{E}_n \cdot \mathbf{E}_m \mathbf{d}\mathbf{x} = 0 \quad (15)$$

or, equivalently, if

$$I_{nm} = \int_{-a}^a \mathbf{H}_n \cdot \mathbf{H}_m \mathbf{d}\mathbf{x} = 0 \quad (16)$$

where \cdot represents the vector dot product.

The modes of the hollow slab are approximately orthogonal, under the assumptions

$$u'' \ll u' \quad (17)$$

$$\eta \ll 1. \quad (18)$$

This can be verified by inserting the field expressions (3) and (4) in (15) or (16).

B. Rough Waveguide

In order to model realistic wall surfaces, we must take into account their roughness. In this section, we consider slab waveguides made of uniform material, but the geometry of the walls is no longer smooth, as shown in Fig. 12.

The analysis of multimoded waveguides and the coupling between the propagating modes started with a series of papers by Marcuse [13]–[18] and was extended by others [19]–[23]. These works analyze a dielectric multimoded optical fiber in order to predict the effects of production imperfections.

The analysis here follows the approach taken by Marcuse [13] to the mode coupling caused by the roughness of the waveguide walls; it relies on the assumption of small perturbations of the wall geometry.

The 2-D model is maintained, where there is no variation in the y direction. The wall boundary near $x = a$ is given by the

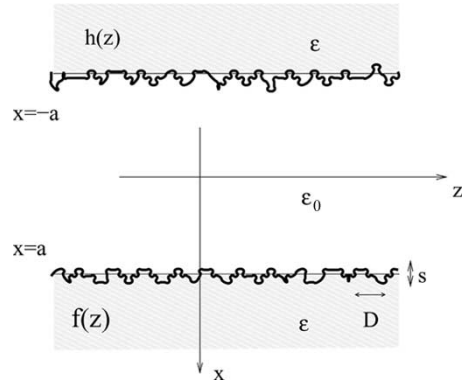


Fig. 12. Rough slab waveguide.

function $x = f(z)$ and the boundary near $x = -a$ is given by $x = h(z)$. We characterize the wall perturbations statistically, using their correlation functions, where we assume that the perturbations on both walls are independent of each other and wide sense stationary, i.e., the statistical properties do not change along the hallway for any point z_0 along the waveguide

$$\langle [f(z_0) - a][f(z_0 + z) - a] \rangle = s^2 e^{-\frac{|z|}{D}} \quad (19)$$

where s is the root-mean square (rms) deviation of the wall from perfect straightness and D is the correlation length. We assume the same statistics for $h(z)$, which defines the deviations of the wall near $x = -a$. The exponential correlation assumption may not be accurate, but it captures two important features of every correlation function, namely a correlation length and a variance.

We now examine the deviation of the complex dielectric constant of the waveguide from the smooth waveguide. Near the boundary $x = a$ this deviation is given by

$$\begin{aligned} \epsilon_r(x, z) - \epsilon_s(x, z) &= \Delta\epsilon(x, z) \quad (20) \\ &= \begin{cases} 0 & \begin{cases} x < a & a < f(z) \\ x < f(z) & f(z) < a \end{cases} \\ 1 - \epsilon & a < x < f(z) \quad a < f(z) \\ -(1 - \epsilon) & f(z) < x < a \quad f(z) < a \\ 0 & \begin{cases} x > f(z) & f(z) > a \\ x > a & a > f(z) \end{cases} \end{cases} \quad (21) \end{aligned}$$

where $\epsilon_r(x, z)$ stands for the relative dielectric constant of the rough waveguide and $\epsilon_s(x, z)$ is defined in (1). The deviation near $x = -a$ is expressed in a similar manner, in terms of $h(z)$.

The fields in the waveguide are solutions of the wave equation

$$\frac{\partial^2 E_y}{\partial x^2} + \frac{\partial^2 E_y}{\partial z^2} + (\epsilon_s(x, z) + \Delta\epsilon(x, z)) \epsilon_0 k^2 E_y = 0. \quad (22)$$

The modes of the smooth waveguide are solutions of

$$\frac{\partial^2 E_y}{\partial x^2} + \frac{\partial^2 E_y}{\partial z^2} + \epsilon_s(x, z) \epsilon_0 k^2 E_y = 0. \quad (23)$$

We express the fields in the perturbed waveguide in terms of the modal fields of the smooth waveguide and manipulate the wave equation to calculate the coupling among the modes. A low coupling assumption is used in the calculation, which means that

the distances characteristic of the coupling process are significantly bigger than the wavelength. After considerable manipulation, the coupling among the modes is expressed by a linear set of coupled power equation

$$\frac{dP_m}{dz} = -\alpha_m P_m + \sqrt{\pi} 2s^2 D \sum_{n=1}^{2N} |K_{mn}|^2 e^{-[\frac{D}{2}(\beta_m - \beta_n)]^2} (P_n - P_m) \quad (24)$$

where $m = 1, \dots, 2N$, P_m is the power carried by the m th mode and

$$K_{mn} = -(\epsilon - 1) \frac{k^2}{2ja} \frac{T_n(u'_n) T_m(u'_m)}{\sqrt{\beta'_n} \sqrt{\beta'_m}} \quad (25)$$

and

$$T_n(v) = \begin{cases} \cos(v) & \begin{cases} 1 \leq n \leq N \\ n \text{ odd, TE symmetric} \end{cases} \\ \sin(v) & \begin{cases} 1 \leq n \leq N \\ n \text{ even, TE antisymmetric} \end{cases} \\ \sin(v) & \begin{cases} N+1 \leq n \leq 2N \\ (n-N) \text{ even, TM symmetric} \end{cases} \\ \cos(v) & \begin{cases} N+1 \leq n \leq 2N \\ (n-N) \text{ odd, TM antisymmetric.} \end{cases} \end{cases} \quad (26)$$

The TE modes are indexed $1, \dots, N$ and the TM modes by $N+1, \dots, 2N$. The variables P_n and β_n with $n > N$ correspond to TM modes with index $n - N$.

The coupling between TE and TM modes is not predicted by the model, because of the 2-D assumption. We include cross polarization coupling in order to compensate for this over-simplification of the model.

α_m are arbitrary modal loss factors. These factors do not emerge from the coupling theory; they are introduced in order to account for physical effects. A natural choice for the loss factors α_m is the modal loss factors β'_m calculated in (10).

The coupled power equations (24) can be expressed as a simple matrix equation, where the unknown is a vector containing the power level of each mode

$$\bar{P} = \begin{pmatrix} P_1 \\ \vdots \\ P_{2N} \end{pmatrix} \quad (27)$$

and the coupled power equation takes the form

$$\frac{\partial \bar{P}}{\partial z} = \Gamma \bar{P} \quad (28)$$

where Γ is an $2N \times 2N$ symmetric matrix which holds all the power coupling coefficients.

1) *Solution of the Coupled Power Equations:* The coupled power equation (28) is easily solved in terms of the eigenvalues and eigenvectors of the coupling matrix Γ

$$\bar{P}(z) = \sum_{n=1}^{2N} \bar{B}_n e^{-\lambda_n z} \quad (29)$$

where \bar{B}_n are the eigenvectors of Γ and λ_n are the corresponding eigenvalues. In order to investigate the steady-state behavior of the solution, we are interested only in the first

(smallest) eigenvalue of Γ , which describes the slowest decrease in power level at growing distances from a source

$$\bar{P}(z) = \bar{B}_1 e^{-\lambda_1 z}. \quad (30)$$

The steady-state solution varies with distance along the hallway, but only via the exponential decay. The distribution of power among the modes does not change along the hallway. The steady-state solutions we calculated tend to concentrate most of the power in the low-order modes.

In addition to our interest in the steady-state solution, we also look at the dynamic behavior of the power measured at small distances from a source. We model the source as a distribution of power among the waveguide modes, and then solve (28) numerically. The results presented in Section II are the total power along the waveguide predicted using this method, where the calculation was performed by the Matlab software.

C. Floor and Ceiling

The introduction of a third spatial dimension into our waveguide model creates considerable complications, so we take here an approximate approach to the effects of the floor and ceiling on the hallway propagation. The floor and ceiling are modeled as smooth surfaces made of very good conductors. Thus, their effects can be considered separately from the effects of the walls.

The hallway can be seen as an intersection between two slab waveguides, one with smooth conducting boundaries (the floor and ceiling) and the other with rough, lossy dielectric boundaries (the walls of the hallway). The effects of these two waveguides can be separated, where the floor-ceiling guide determines the y dependence of the field components and the wall guide determines the x dependence. Using this coordinate separation model, there is only a minor effect of the floor and ceiling on the behavior of the fields and the coupling among the modes. The results shown in Section IV were calculated with the 2-D model.

D. Hallway Junction Model

This section describes the model of hallway junctions, where power flows along one hallway (the "main" hallway) into another ("side") hallway. The prediction of power levels along the side hallway is an important strength of the waveguide model; this section discusses the intersection between the waveguides representing the hallways, that is used to calculate the initial conditions for the side hallway. We present here an intuitive explanation of the mode coupling mechanism. For a more thorough analysis see [24] and [25].

In order to look at the coupling mechanism in some detail, we consider the plane wave decomposition of the modes. Each mode can be decomposed into a pair of plane waves propagating at equally oblique angles with the z direction. The lower order modes are decomposed into plane waves that propagate in an almost parallel direction to the z axis. High-order modes travel in directions increasingly oblique to the z axis. When considering a perpendicular hallway corner, the low-order modes in the main hallway couple into high-order modes in the side hallway and *vice versa* (Fig. 13).

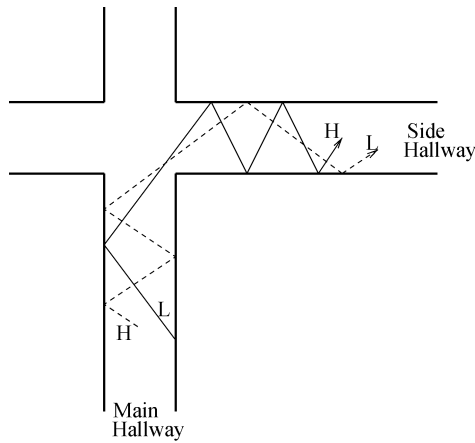


Fig. 13. Hallway corner model. The solid line represents a low-order mode of the main hallway coupled into a high-order mode of the side hallway. The dashed line represents a high-order mode of the main hallway coupled into a low-order mode of the side hallway.

We assume steady-state distribution of power of the modes in the main hallway, where most of the power is contained in the low order modes. As a consequence, the power coupled into the side hallway is mostly contained in the high-order modes. The power leaking into the side hallway is redistributed among the modes as it propagates along the hallway.

The expected effect in the side hallway is a significant decrease of power level as the receiver moves away from the junction. At a certain distance, where the modal distribution of power reaches its steady state, the decrease of power loss along the hallway resumes its steady-state rate.

The model assumes solid walls, so it does not present leakage between the hallways through the rooms. In reality, this leakage may be significant.

IV. DISCUSSION

The measurements along and near the hallways (Figs. 6 and 8–10) show that when the receiver is 10 m or further from the transmitter, power levels are usually stronger in the hallway than in the adjacent rooms. This is true even when the rooms are closer to the transmitter (as in the case of Hallway 6). The power levels in the rooms may be higher than those of the hallway, in cases where the direct propagation from the transmitter to the rooms is normally incident on the intermediate walls. This is shown for Hallway 3 (Fig. 10), for positive y .

The dominance of the hallway propagation over direct propagation through the walls is also clear when examining the power levels in hallway junctions.

Coupled modal theory predicts that for radiation along a hallway, the low-order TE modes dominate at large distances, and that a steady-state rate of power loss is reached beyond an initial high-loss area near the source. The dominance of the lowest order mode is seen in Fig. 7, where the electric field shape across the hallway is shown. The field is stronger in the middle of the hallway for sufficient distance from the transmitter. The theory predicts that the uniform distribution near the transmitter transforms to a field dominated by the low-order modes at further distances. Simulation with the parameters that appear to characterize the Packard building

(hallways 1.8 m wide, walls with $\epsilon = 3$, $\sigma = 0.035$ S/m, $D = 2$ m and $s^2 = 0.2$ m²) shows that the steady-state power distribution among the waveguide modes has almost all the power in the lowest order TE mode. The evolution from a uniform power distribution (over the modes) to the steady state one occurs over 5 m.

Measurements in a different building show that the capacity of multiple antenna (MIMO) systems diminishes along indoor hallways [26]. This phenomenon is intimately related with the convergence of the power distribution to the steady state one, and the accompanying loss of degrees of freedom in the channel. If all the power is concentrated in a single mode then the multiple antenna advantage cannot be utilized because of the low rank of the propagation channel. The capacity decreases as the transmitter and receiver move away from each other, as the coupling among the modes reduces the number of degrees of freedom of the channel.

Fig. 6 shows the measurements in Hallway 1, with the theoretical prediction for average power levels, based on modal theory, where the initial power distribution (over the modes) described a narrow TE source in the middle of the hallway.

Figs. 8–10 show power measurements in Hallways 3, 5, and 6, together with the theoretical prediction based on the waveguide model with uniform initial distribution. The model predicts a significant change in the distribution of power, when the receiver turns from one hallway to another. We used a uniform distribution of power over the modes as initial conditions after turning a corner. The power level used after turning a corner was determined in the simulation from the power level calculated for the intersecting hallway. In junctions where the main hallway (that guides power into the junction) continues after the intersection, such as in a full (cross) junction, the power level at the cross hallway is half (−3 dB) of the main hallway level. In junctions where the main hallway ends (such as a corner), the power initializing the side hallway equals the power at the main hallway.

The power levels in the rooms adjacent to the hallways are deduced in the model from the penetration of the different modes through the walls. We note that this model considers only the hallway guiding effects, so it omits direct radiation from the transmitter.

The penetration from a hallway to the adjacent rooms varies along the hallway, because the power distribution among the modes changes. The high-order modes penetrate strongly into the walls, and they tend to be strong near the transmitter and hallway junctions, whereas the low order modes, that do not penetrate as well, dominate in the steady state power distribution.

The calculation of the rooms’ levels is based on the penetration of the different modes through the hallway walls. The penetration was calculated using the formulas for oblique incidence of plane waves on an infinite half space made of uniform material with $\epsilon = 3$ and $\sigma = 0.035$ S/m [9]. The predicted power level in the rooms is 9 dB below the hallway levels, when the hallway power distribution is at steady state. This prediction is too high for Hallway 1 (Fig. 6), but too low in Hallways 5 and 6 (Figs. 8 and 9). It appears that the simple model is insufficient in describing the room power levels.

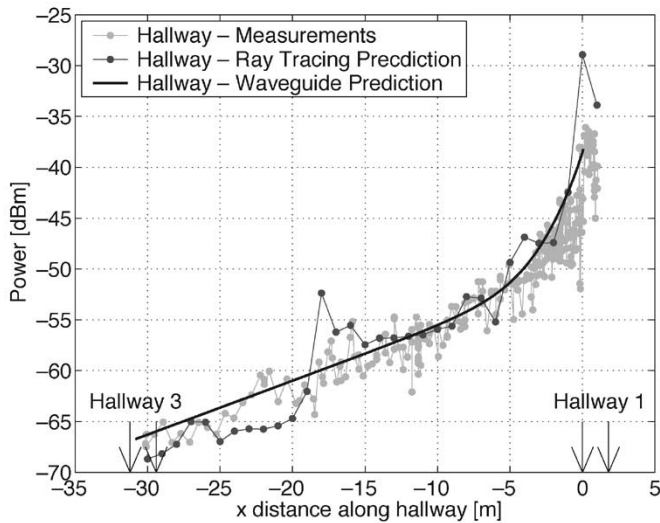


Fig. 14. Median power in Hallway 5, with predictions of the waveguide model and the WiSE ray tracing tool. The geometry is shown in Fig. 2.

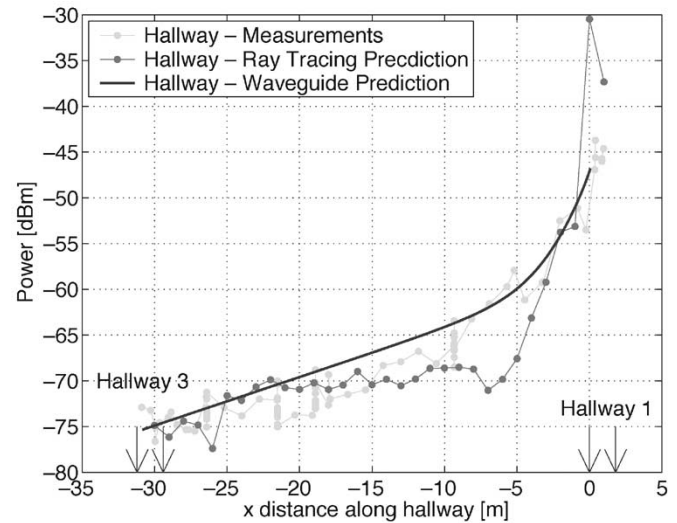


Fig. 15. Median power in Hallway 6, with predictions of the waveguide model and the WiSE ray tracing tool. The geometry is shown in Fig. 2.

A. Comparison With Ray Tracing

This section presents a comparison of the waveguide power level prediction with that calculated using the WiSE ray tracing software Version 19¹ [27]. The ray tracing software required a detailed description of the building; the locations of all the inner and outer walls were specified, as well as their construction material. The input to the ray tracing tool was an order of magnitude larger (in memory requirements) and considerably more complicated than the input of the waveguide model.

The ray tracing calculation is much more complex than the waveguide model, this was evident in the amount of run time for the two models. The ray tracing tool produced the results shown here after about two hours of calculation on a modern desktop; the waveguide model implemented in Matlab required about 1 min on the same computer. We note the ray tracing tool predicted the power levels across the whole basement, where the waveguide model predicted power levels only in the hallways and adjacent rooms.

The ray tracing complexity is affected by the choice of parameters of the model, namely the maximum numbers of bounces and diffractions for each ray. After some experimentation with the tool it appeared that four bounces and two diffractions were necessary to provide reasonable output accuracy of the ray tracing prediction.

Other parameters used for the ray tracing calculations were as follows (many parameters are not specified here as they were left at their default values):

- 1) 2-D ray tracing with ground reflections (2-D pincushion prediction);
- 2) ray magnitudes were summed to predict power (rather than summing powers);
- 3) receiver grid 1 m × 1 m across the whole basement;
- 4) frequency 900 MHz;

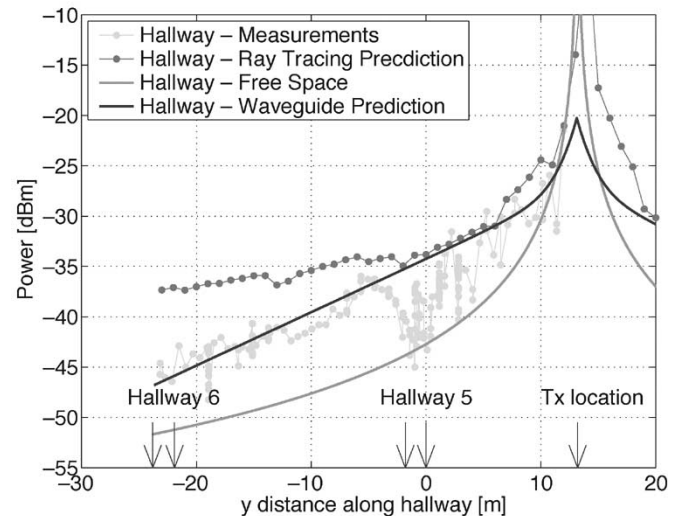


Fig. 16. Median power in Hallway 1, with predictions of three models: the waveguide model, the WiSE ray tracing tool, and free space. The geometry is shown in Fig. 2.

- 5) transmitter power 34 dBm, with ray power threshold -100 dBm.

The ray tracing tool provides good predictions for Hallways 5 and 6 (Figs. 14 and 15), similar to the waveguide model predictions. The ray tracing prediction is not accurate in Hallway 1 (Fig. 16), which is the line of sight hallway.

In Hallway 3, which is farthest from the transmitter, the ray tracing tool fails to capture the 8-dB increase of power level at the intersection with Hallway 5 and its predicted power level has a peak in the area closest to the transmitter (Fig. 17). The prediction in this hallway is not accurate for the waveguide model as well, but this model does show the increased power level at the intersection. The measurements in Hallway 3 were done close to the sensitivity limit of the equipment, so the actual power levels may be lower than those shown in Fig. 17.

¹Lucent Technologies WiSE Software Tool, <http://www.bell-labs.com/org/wireless/wisext.html>.

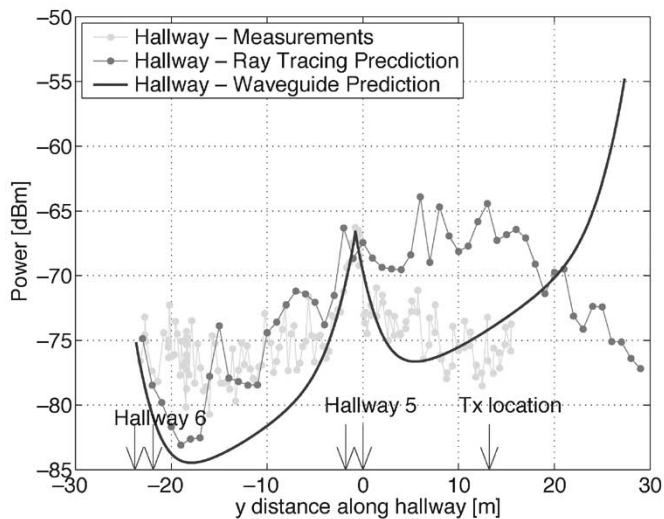


Fig. 17. Median power in Hallway 3, with predictions of the waveguide model and the WiSE ray tracing tool. The geometry is shown in Fig. 2.

In summary, the ray tracing tool and the waveguide model provide comparable predictions, with two orders of magnitude higher complexity for the ray tracing. Both models show good predictions in hallways one corner away from the transmitter. The prediction of power levels in the line of sight hallway is done more accurately by the waveguide model. In a hallway that is remote from the transmitter both models fail to give an accurate prediction, but the waveguide model shows a pattern near the intersection that is similar to the measured one.

The advantage offered by the ray tracing tool over the waveguide model is versatility: ray tracing is not limited to any geometry and no assumptions need be made on the construction materials. The main drawback of the ray tracing tool is its complexity. The waveguide model on the other hand works only for specific geometries, but it requires a simple input and runs with low complexity.

V. CONCLUSION

This paper presented a new model for UHF propagation in large buildings, based on the guiding effects of hallways. The importance of the guiding mechanism was shown by comparing hallway and room power levels in an office building. The hallway power levels are higher in most cases, even when the hallway is further from the transmitter than the rooms. The model is based on the waveguide analysis of the hallways, where the roughness of the walls causes mode coupling which is analyzed in an average manner. The steady-state distribution of power over the modes has most of the power in the lowest order TE mode. The evolution of the power distribution from the area of the transmitter or a junction, along the hallway, explains the sharp decrease of power levels near these areas, which evolves into a lower rate of power loss. The model suggests an intuitive explanation of the propagation mechanism, which is absent in other commonly used propagation models. It offers a simple alternative to ray tracing, that gives accurate power level predictions while requiring a simple input and very little computer resources.

ACKNOWLEDGMENT

The authors would like to thank Lucent Technologies for use of the WiSE software tool (educational version) for comparison to our model (Section IV-A), and J. Ling and R. Valenzuela for sending the software and helping with the setup.

REFERENCES

- [1] H. L. Bertoni, W. Honcharenko, L. R. Maciel, and H. H. Xia, "UHF propagation prediction for wireless personal communications," *Proc. IEEE*, vol. 82, pp. 1333–1359, Sept. 1994.
- [2] U. Dersch and E. Zollinger, "Propagation mechanisms in microcell and indoor environment," *IEEE Trans. Veh. Technol.*, vol. 43, pp. 1058–1066, Nov. 1994.
- [3] R. Valenzuela, "A ray tracing approach to predicting indoor wireless transmission," in *Proc. Vehicular Technology Conf.*, 1993, pp. 214–218.
- [4] J.-F. Lafortune and M. Lecours, "Measurement and modeling of propagation losses in a building at 900 MHz," *IEEE Trans. Veh. Technol.*, vol. 39, pp. 101–108, May 1990.
- [5] T. S. Rappaport, *Wireless Communications Principles and Practices*. Englewood Cliffs, NJ: Prentice Hall, 1996.
- [6] P. Kyritsi and D. C. Cox, "Modal analysis of MIMO capacity in a hallway," in *Proc. IEEE Global Telecommunications Conf.*, vol. 1, 2001, pp. 567–571.
- [7] W. C. Stone, "Electromagnetic signal attenuation in construction materials," NIST Construction Automation Prog. Rep. no. 3, Tech. Rep. NISTIR 6055, Oct. 1997.
- [8] S. Kim, B. Bougerolles, and H. L. Bertoni, "Transmission and reflection properties of interior walls," in *Proc. IEEE Int. Conf. Personal Communications*, Sept. 1994, pp. 124–128.
- [9] D. Porrat, "Radio propagation in hallways and street for UHF communications," Ph.D. dissertation, Stanford Univ., Stanford, CA, 2002.
- [10] B. Adam and F. Kneubühl, "Transversely excited 337 μm HCN waveguide laser," *Appl. Phys.*, vol. 8, no. 4, pp. 281–291, Dec. 1975.
- [11] J. J. Burke, "Propagation constants of resonant waves on homogeneous, isotropic slab waveguides," *Appl. Opt.*, vol. 9, no. 11, pp. 2444–2452, Nov. 1970.
- [12] O. Landron, M. J. Feuerstein, and T. S. Rappaport, "A comparison of theoretical and empirical reflection coefficients for typical exterior wall surfaces in a mobile radio environment," *IEEE Trans. Antennas Propagat.*, vol. 44, pp. 341–351, Mar. 1996.
- [13] D. Marcuse, "Mode conversion caused by surface imperfections of a dielectric slab waveguide," *Bell Syst. Tech. J.*, pp. 3187–3215, Dec. 1969.
- [14] —, "Radiation losses of dielectric waveguides in terms of the power spectrum of the wall distortion function," *Bell Syst. Tech. J.*, pp. 3233–3242, Dec. 1969.
- [15] —, "Derivation of coupled power equations," *Bell Syst. Tech. J.*, vol. 51, no. 1, pp. 229–237, Jan. 1972.
- [16] —, "Power distributions and radiation losses in multimode dielectric slab waveguides," *Bell Syst. Tech. J.*, vol. 51, no. 2, pp. 429–454, Feb. 1972.
- [17] —, "Fluctuations of the power of coupled modes," *Bell Syst. Tech. J.*, vol. 51, no. 8, pp. 1793–1800, Oct. 1972.
- [18] —, "Higher-order loss processes and the loss penalty of multimode operation," *Bell Syst. Tech. J.*, vol. 51, no. 8, pp. 1819–1836, Oct. 1972.
- [19] B. Crosignani, C. H. Papas, and P. Di Porto, "Theory of time-dependent propagation in multimode lightguides," *J. Opt. Soc. Amer.*, vol. 67, no. 10, pp. 1300–1307, Oct. 1977.
- [20] W. E. Kohler, "Propagation in a randomly perturbed multimode matched waveguide," *Wave Motion*, vol. 4, pp. 243–263, 1982.
- [21] G. Cancillieri and P. Fantini, "Mode coupling effects in optical fibers: Perturbative solution of the time-dependent power flow equation," *Opt. Quantum Electron.*, vol. 15, pp. 119–136, 1983.
- [22] D. G. Hall, "In-phase scattering in planar optical waveguides: Refractive-index fluctuations and surface roughness," *J. Opt. Soc. Amer. A*, vol. 2, no. 5, pp. 747–752, May 1985.
- [23] D. Swirck and A. Heimrath, "Random multimode optical media: I. Mode coupling process in slab waveguide with stochastic wall perturbations," *J. Mod. Opt.*, vol. 39, no. 4, pp. 681–688, 1992.
- [24] N. Blaunstein, *Radio Propagation in Cellular Networks*. Norwood, MA: Artech House, 2000.

- [25] J. Lee and H. L. Bertoni, "Coupling at L, T and cross junctions in tunnels and urban street canyons," in *Proc. IEEE Vehicular Technology Conf.*, vol. 1, Spring 2001, pp. 274–278.
- [26] D. Porrat, P. Kyritsi, and D. C. Cox, "MIMO capacity in hallways and adjacent rooms," in *Proc. IEEE Globecom*, Nov. 2002, pp. 1930–1934.
- [27] S. J. Fortune, D. M. Gay, B. W. Kernighan, O. Landron, R. A. Valenzuela, and M. H. Wright, "WISE design of indoor wireless systems: practical computation and optimization," *IEEE Computat. Sci. Eng.*, vol. 2, no. 1, pp. 58–68, Spring 1995.



Dana Porrat received the B.S. degree in electrical engineering from the Technion, Haifa, Israel, in 1992, the M.S. degree from Tel Aviv University, Tel Aviv, Israel, in 1997, and the Ph.D. degree in electrical engineering from Stanford University, Stanford, CA, in 2002.

She is currently with the University of California at Berkeley, where she is working on the information theoretic aspects of ultrawide-band communication.

Donald C. Cox (M'61–SM'72–F'79) received the B.S. and M.S. degrees in electrical engineering from the University of Nebraska, Lincoln, in 1959 and 1960, respectively, and the Ph.D. degree in electrical engineering from Stanford University, Stanford, CA, in 1968. He received an Honorary Dr.Sci. degree from the University of Nebraska in 1983.

From 1960 to 1963, he was with Wright-Patterson AFB, OH, where he researched microwave communications system design. From 1963 to 1968, he was with Stanford University researching tunnel diode amplifier design and research on microwave propagation in the troposphere. From 1968 to 1973, his research at Bell Laboratories, Holmdel, NJ, in mobile radio propagation and on high-capacity mobile radio systems provided important input to early cellular mobile radio system development, and is continuing to contribute to the evolution of digital cellular radio, wireless personal communications systems, and cordless telephones. From 1973 to 1983, he was Supervisor of a group at Bell Laboratories that did innovative propagation and system research for millimeter-wave satellite communications. In 1978, he pioneered radio system and propagation research for low-power wireless personal communications systems. At Bell Laboratories in 1983, he organized and became Head of the Radio and Satellite Systems Research Department that became a Division in Bell Communications Research (Bellcore) with the breakup of the Bell System on January 1, 1984. He was Division Manager of the Radio Research Division until it again became a department in 1991. He continued as Executive Director of the Radio Research Department where he championed, led, and contributed to research on all aspects of low-power wireless personal communications entitled Universal Digital Portable Communications (UDPC). He was instrumental in evolving the extensive research results into specifications that became the U.S. Standard for the Wireless or Personal Access Communications System (WACS or PACS). In September 1993, he became a Professor of Electrical Engineering and Director of the Center for Telecommunications, Stanford University, where he continues to pursue research and teaching of wireless mobile and personal communications. He was appointed Harald Trap Friis Professor of Engineering at Stanford in 1994. He is author or coauthor of many papers and conference presentations, including many invited and several keynote addresses, and books. He has been granted 15 patents.

Dr. Cox was a member of the Administrative Committee of the IEEE Antennas and Propagation Society (1986–1988), and was an Associate Editor of the *IEEE TRANSACTIONS ON ANTENNAS AND PROPAGATION* (1983–1986). He received the 1983 IEEE Vehicular Technology Society Paper of the Year Award, the IEEE 1985 Morris E. Leeds Award, the 1990 Communications Magazine Prize Paper Award, the IEEE Communications Society 1992 L. G. Abraham Prize Paper Award, the IEEE 1993 Alexander Graham Bell Medal "for pioneering and leadership in personal portable communications," and the IEEE Third Millennium Medal in 2000. He was also a corecipient of the 1983 International Marconi Prize in Electromagnetic Wave Propagation (Italy), and received the Bellcore Fellow Award in 1991. He is a Fellow of AAAS and the Radio Club of America and a member of the National Academy of Engineering, Commissions B, C and F of USNC/URSI, Sigma Xi, Sigma Tau, Eta Kappa Nu, and Phi Mu Epsilon. He was a member of the URSI Intercommission Group on Time Domain Waveform Measurements from 1982 to 1984. He is a Registered Professional Engineer in Ohio and Nebraska.